WEP Warwick Evans Publishing

International Journal of Natural Resources and Environmental Studies

ISSN: 3006-2012 (Print), ISSN: 3006-0834 (Online) | Volume 8, Number 3, Year 2026
DOI: https://doi.org/10.62051/ijnres.v8n3.06
Journal homepage: https://wepub.org/index.php/IJNRES/index

Application of First Break Tomography Technology in Shallow Loess Layer Detection

Chi Wang[1, 2]

[1] School of Earth Sciences and Engineering, Xi'an Shiyou University, Xi'an, China
[2]Shaanxi Key Laboratory of Petroleum Accumulation Geology, Xi'an Shiyou University, Xi'an, China

ABSTRACT

The near-surface structure and unique physical properties of loess-covered areas render traditional geophysical methods ineffective in achieving high-precision structural detection of loess layers, thereby restricting regional resource exploration, geological hazard prevention, and optimal utilization of water resources. Focusing on the loess layers in the Qianyang area, this study aims to address the challenge of fine characterization of loess layer structures using first-break tomographic imaging technology. Firstly, the key parameters such as vertical stratification and velocity of loess layer are obtained through the investigation and analysis of geological data, and the initial geological geophysical model is constructed; Then, typical models such as horizontal surface, undulating surface and fault are designed to carry out forward simulation, analyze the influence of terrain and fault on first break propagation, and verify the applicability of first break tomography technology; Finally, the tomographic inversion of the actual data in the study area is carried out, and the comprehensive interpretation is completed by combining the seismic reflection profile. The results indicate that topographic relief causes regional shifts in first-break travel times, while faults induce first-break signal anomalies. However, first-break tomographic imaging technology can effectively mitigate these effects, enabling accurate identification of key geological interfaces such as the internal structures of individual loess layers, loess-bedrock interfaces, and concealed faults, among others. This study confirms the effectiveness of first-break tomographic imaging technology for delineating loess layer structures.

KEYWORDS

Loess Overburden; First Break Forward Simulation; Tomography.

1. INTRODUCTION

Loess tablelands are typical geomorphic units of the Loess Plateau in China, which are widely distributed in the Ordos Basin, the southwestern Tarim Basin, and other regions. Loess tablelands in the Ordos Basin account for approximately 72.4% of the total loess area in China and have developed the most representative loess geomorphic sequences globally[1]. This region is not only a key enrichment belt for China's energy and mineral resources but also sustains intensive agricultural, industrial, and human activities. Coal, oil, natural gas, and various mineral resources mostly occur in the bedrock beneath the thick loess cover. However, the loess layer exhibits special physical properties, such as loose structure, well-developed vertical joints, high porosity, and strong physical heterogeneity, resulting in severe attenuation of the energy of seismic and electromagnetic waves. Traditional geophysical methods face challenges in detecting bedrock interfaces and resource occurrence states[2-3]. In addition, geological disasters such as surface subsidence, landslides, and collapses—triggered by loess collapsibility—occur frequently; when coupled with the reality of regional water resource shortage, this has severely constrained regional sustainable development[4].

Therefore, conducting high-precision detection of the loess cover structure and clarifying the spatial distribution and thickness variations of collapsible loess are of great significance for resource exploration, disaster prevention, and water resource management.

At present, the Loess exploration is mainly based on geophysical methods such as gravity, electromagnetic, reflected seismic and surface wave, but most of the research still focuses on the analysis of middle and deep structure[5-8]. Moreover, because the loess layer has the characteristics of low speed, thick layer, strong attenuation and serious absorption of seismic and electromagnetic signals, there are still obvious deficiencies in the high-precision imaging of near surface structures, especially shallow stratification, lateral heterogeneity and bottom interface morphology. The first break tomography method is based on the travel time information of direct wave and refracted wave. With the help of high-density observation system and continuous medium inversion ability, it can effectively overcome the limitations of traditional exploration methods in loess area. This method has been widely used in the study of near surface structure in recent years[9-14]. Through multi-scale velocity modeling and dynamic constraint optimization, a more accurate formation model can be established. For the detection of shallow loess layer structure, this paper takes the loess layer in Qianyang area as the research object, and systematically evaluates the applicability of first break tomography in loess region by constructing a typical loess geological model; Based on this technology, a high-precision shallow velocity model is constructed to accurately depict the spatial distribution characteristics of the loess layer, trying to provide a basis for geological disaster risk assessment, engineering foundation stability evaluation and underground resource exploration in the loess region.

2. GEOLOGICAL BACKGROUND

The Qianyang Area is located in the southern part of the Loess Plateau, at the junction zone of the Qinling Orogenic Belt and the Qilian Orogenic Belt, while also linking the southwestern margin of the Ordos Basin and the Western Uplift of the Weihe Basin (Fig. 1a) (Fig.1a) [15]. This unique geographical location makes it a typical area for studying the interactions between the Loess Plateau and several key geological units. As the world's largest loess sedimentary area, the Loess Plateau interacts with geological units such as the Qinling Mountains and the Ordos Basin, resulting in complex and diverse geological evolution processes[16] .

From the perspective of geomorphic features, Qianyang area presents a significant ternary structure (Fig.1b). In the south is the uplift zone of Qinling Mountains with high terrain and crisscross mountains, which is an important boundary of regional topography; The northern part belongs to the tableland landform of the western extension of the Loess Plateau. The loess is widely covered, accounting for about 70% of the total area of the region. The soil here is mainly composed of Malan loess, Lishi loess and Wucheng loess, recording the deposition process in a long geological history; The middle part is a valley terrace system formed by the alluvial deposits of the Weihe River. The terrain is low, flat and open, with an average altitude of 1320 meters. In terms of geological tectonic units, Qianyang area mainly includes three major components. The high terrace on the North Bank of the Weihe basin, namely the Quaternary loess tableland, is an important area for loess accumulation and river terrace development; The fold uplift tectonic belt in the southwestern margin of Ordos Basin, namely Weibei uplift, has undergone many tectonic movements. Its geological structure is complex and the transition area in the southern margin of Ordos Basin is connected with different geological tectonic units, which plays a key transitional role in the process of geological evolution[17-18].

The loess sedimentary layers in the study area are in direct contact with the underlying Mesozoic stratigraphy. This unique stratigraphic relationship provides a key clue for studying the sedimentary evolution and tectonics of loess in China. Through the investigation and analysis of parameters such as surface structure, lithology, and velocity in the study area[19-24], the surface of typical loess source areas can be divided into four layers, namely the weathered layer, low-velocity layer, velocity-reducing layer, and high-velocity layer from top to bottom. With respect to the water content of the surface layer, the loess can be further divided into three layers: dry loess, moist loess, and water-bearing loess, in order from top to bottom, followed by bedrock. Owing to differences in the physical properties of different strata, their physical property parameters also inevitably vary according to surveys (Table 1), which provides a prerequisite for solving geological problems in this field using geophysical exploration methods.

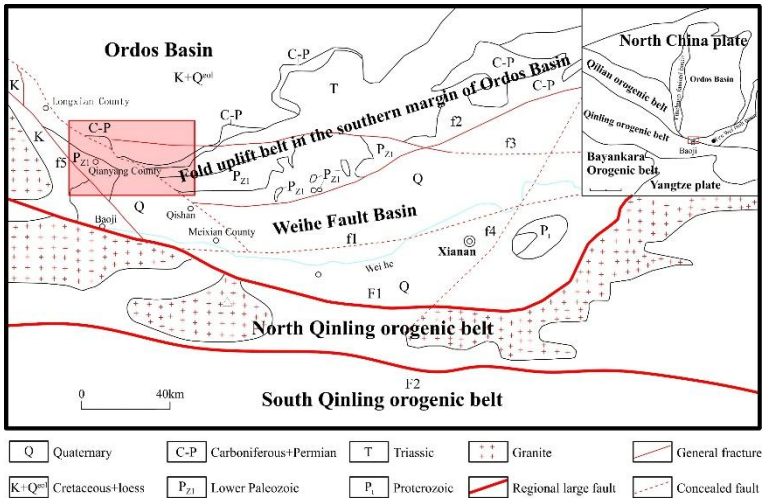

(a) The main Geological Structure Map of the Study Area (revised according to Yujiang River, 2018), and the red box is the study area

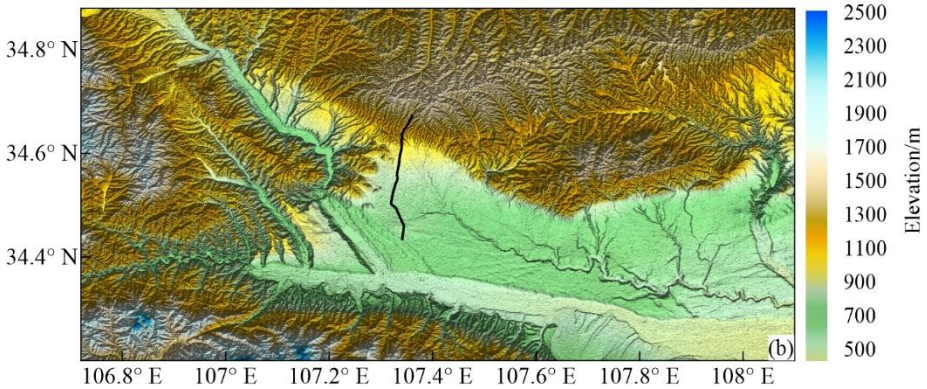

(b) Topographic Map of the Study Area

Fig. 1 Geological Structure Distribution in the Study Area

Table 1 physical parameters of loess stratum

Stratum	Lithology	vP(m/s)	vS(m/s)	ρ(g/cm³)
Dry loess	Malan loess and Holocene Loess	300~600	100~300	1.3~1.59
Wet loess	Lishi loess	800~1200	300~500	1.6~1.79
Mastic	Wucheng loess	1500~1800	600~1000	1.8~2.1
Bedrock	Saturated argillaceous sandstone and unsaturated argillaceous sandstone	2000~3000	1200~1800	2.2~2.5
	Shale and granite	≥3500	≥1800	2.3~2.7

3. DATA AND METHODS

In this study, the technical route of combining seismic forward modeling and first break tomography is used to systematically analyze the near surface structural characteristics of loess covered area. Firstly, the key parameters such as vertical stratification and wave velocity of loess layer are obtained based on geological survey data, and the initial geological geophysical model is established; Then, a variety of typical theoretical models of horizontal surface, undulating surface and fault are designed to carry out forward modeling of seismic wave field. Seismic forward modeling simplifies the geological structure into a digital model containing physical parameters such as velocity and density, selects viscoelastic wave equation for forward modeling according to the characteristics of shallow heterogeneous loess layer in the Loess Plateau, and calculates the quality factor Q value[26] based on empirical formula (formula 1), so as to more truly reflect the attenuation characteristics of seismic waves in loess, and realize the numerical simulation and analysis of wave field propagation characteristics in underground loess layer. Through forward modeling of synthetic seismic records, the influence of the structure of Rehmannia glutinosa soil layer on the propagation of first break waves is revealed.

$$Q \approx 3.516 \times v_P^{2.2} \times 10^{-6} \tag{1}$$

Where vP is the longitudinal wave velocity.

Based on the forward modeling data, the first break tomography method is further used to inverse the velocity structure of shallow loess. First break tomography is a mature geophysical inversion technology, which reconstructs the velocity structure of underground media based on the first break travel time data of seismic waves. Based on the arrival information of the first break from the source to the receiver, the method constructs a high-precision velocity model of the shallow crust through mathematical modeling and iterative inversion. The basic implementation process includes three core steps: first, the underground medium is discretized into a uniform velocity grid and the initial model is constructed; Secondly, the forward algorithm is used to calculate the theoretical travel time and ray path, and compared with the actual observation travel time, and the residual error is used to correct the velocity model; Finally, the model parameters are optimized through multiple iterations until the theoretical travel time and the observed data reach the predetermined fitting accuracy. The mathematical expression of the first break travel time is:

$$T = \sum_{i=1}^{N} p_i d_i \tag{2}$$

Where, T is the travel time from the source to the geophone, pi is the slowness of the i grid (the reciprocal of the velocity), di is the path length of the ray in the grid, and N is the total number of grids through which the ray passes.

In practical application, the multi ray paths formed by a large number of shot detector pairs form a linear equation group, and the velocity values of each grid need to be solved by numerical algorithm to finally generate the velocity contour map. In this paper, the "flat" grid modeling based on the wave equation is realized by using the wavefront tracking method (FMM) and wavelet transform nonlinear iterative inversion algorithm. The FMM method supports fine grid rectangular modeling by efficiently simulating the wavefront propagation path, which significantly improves the computational efficiency and longitudinal resolution; The combination of wavelet transform and nonlinear inversion strategy can search for the optimal solution in the global range, reduce the dependence on the initial model, and is especially suitable for fine modeling of complex structural areas such as the Loess Plateau and fold belt[27-28]. The processing flow mainly includes four links: data preprocessing,first break picking, forward modeling and tomographic inversion (Fig.2).

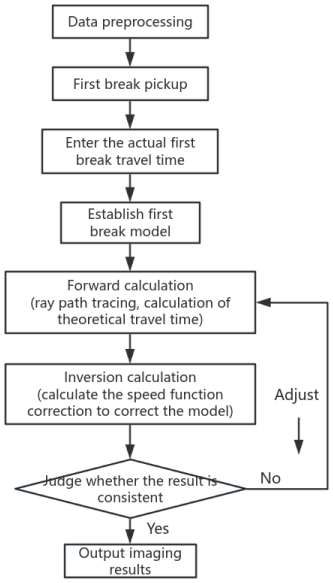

Fig. 2 Basic Flow Chart of First Break Tomography Inversion

4. FORWARD MODELING AND APPLICATION ANALYSIS

4.1. Forward Simulation Analysis

4.1.1. Horizontal and Undulating Surface Model

Loess-covered areas exhibit significant topographic relief. Not only is the overburden thickness substantial, but the near-surface velocity also varies drastically—with surface elevation differences being particularly prominent. When topographic relief exists, seismic waves, after originating from the source, frequently encounter surface interfaces at different elevations during propagation. This phenomenon directly causes complex deflection of seismic wave propagation paths and significant changes in traveltime[29].

To systematically analyze the influence of the aforementioned characteristics on seismic wave propagation, a horizontal-interface model and a relief-interface model (Fig. 3a, b) were established respectively based on survey data (Table 1). The model spans 3000 m in the horizontal direction and 400 m in the vertical direction, a range that fully encompasses the main loess layers and part of the underlying bedrock, with specific parameters provided in Table 2; among these, the maximum elevation difference of the relief model reaches 30 m. For the established geological models, a split-spread acquisition geometry with shots fired at the center was adopted, featuring a shot spacing of 50 m, 281 receiving traces, a trace spacing of 5 m, a 35 Hz Ricker wavelet as the source wavelet, and a sampling interval of 1 ms. Through forward modeling, a total of 32 shot gathers were generated.

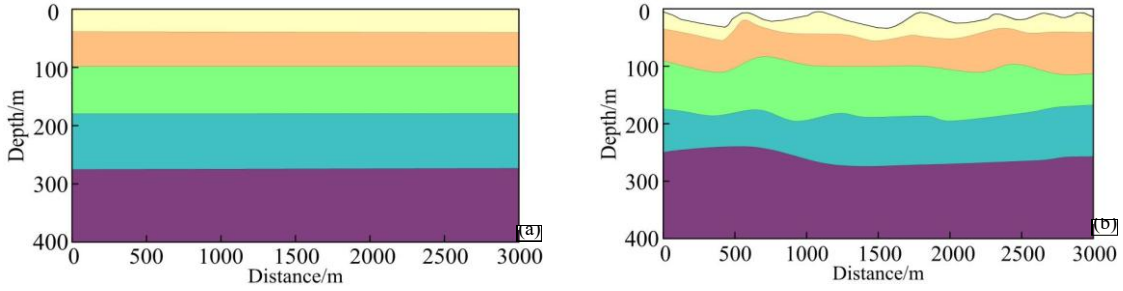

(a) Horizontal Surface Model **(b)** Undulating Surface Model

Fig. 3 Seismic Geological Model

Table 2 Parameters of Seismic Geological Model

Number of layers	vP(m/s)	vS(m/s)	ρ(g/cm³)	Qp	Qs	H(m)
1	500	240	1.4	3	1	40
2	800	370	1.7	9	2	60
3	1600	900	1.9	39	11	80
4	2500	1450	2.2	105	31	100
5	3500	2020	2.6	220	65	

By comparing the single-shot seismic forward modeling results (Fig. 4), it can be observed that the single-shot first-break waves on the loess surface exhibit varying degrees of distortion and stratified characteristics. In terms of propagation time, under undulating surface conditions, the arrival times of first-break waves at different receiving points differ. When the source is located at a higher elevation (trace numbers 180–200) and the receivers are at lower elevations, the seismic wave propagation paths are relatively short, resulting in earlier first-break arrival times; conversely, when the source is at a lower elevation (trace numbers 40–60) and the receivers are at higher elevations, the seismic wave propagation paths lengthen, leading to delayed first-break arrival times. This time discrepancy causes traveltime distortion of first-break waves in seismic records. The forward modeling results indicate that in flat-surface areas, the traveltimes of first-break waves are relatively uniform, and their propagation paths are approximately straight lines; in undulating-surface areas, however, the traveltimes of first-break waves show significant differences, and their propagation paths exhibit complex bending and refraction patterns.

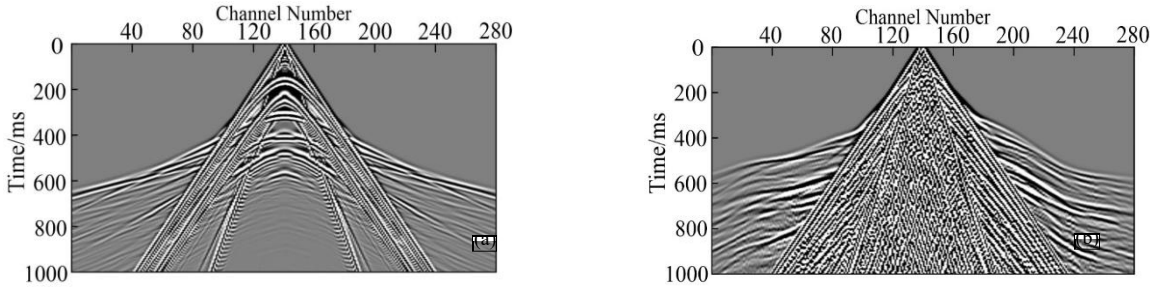

(a) 12th Shot Seismic Record of Horizontal Surface Model

(b) 12th Shot Seismic Record of Undulating Surface Model

Fig. 4 Composite Diagram of Single Shot Seismic Records of Horizontal and Fluctuating Forward Modeling

Building on the above simulation results, further research on the applicability of first-break tomography was conducted. By performing tomographic inversion on the seismic records obtained from forward modeling, the applicability of this method for loess layer stratification under both horizontal and undulating interface conditions in Loess Plateau areas was verified. Seismic records generated via forward modeling of the established horizontal and undulating models were processed using first-break tomography to derive the velocity structure (Fig. 5). In the inversion image of the horizontal-surface model, the horizons are clear and continuous, with relatively uniform velocity distribution and high consistency with the geological model-this confirms the reliability of first-break tomography under relatively simple topographic conditions. The inversion results of the undulating-surface model are also accurate: although the propagation path of first-break waves is complex due to topographic influences, tomography can still accurately reconstruct the underground horizons and velocity information. In the velocity section, while the horizons exhibit some distortion caused by topographic relief, their overall morphology and positions are largely consistent with the actual model. Further analysis of the inversion results reveals that first-break tomography possesses excellent resolution capability for different geological structures beneath undulating surfaces. At the interface between the shallow loess layer and the underlying bedrock, the inversion results clearly depict the undulating morphology of the interface; moreover, the variations in velocity values align with the

lithological characteristics of the strata (i.e., the loess layer has relatively low velocity, while the bedrock has relatively high velocity). This provides a robust basis for more detailed geological structure interpretation in Loess Plateau areas.

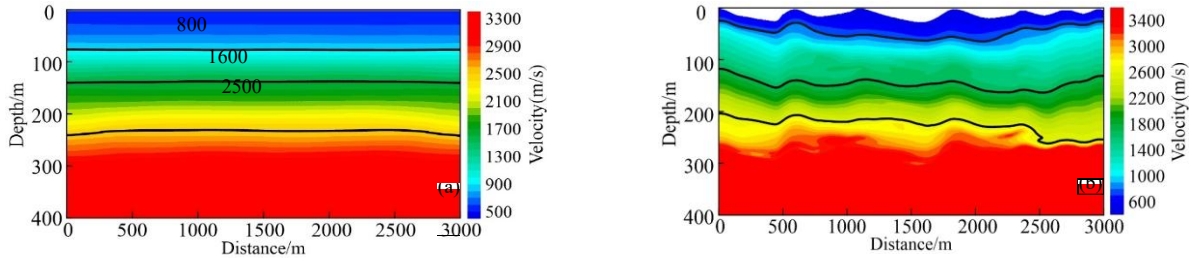

(a) Horizontal Surface Tomographic Inversion Structure

(b) Undulating Surface Tomographic Inversion Structure

Fig. 5 Tomographic Inversion Results of Horizontal and Undulating Surface

4.1.2. Fault simulation

The study area contains multiple concealed faults, with complex geological conditions. To investigate the influence of shallow loess faults on first-break wave propagation patterns and tomography results, a fault geological model was established for analysis during the model construction process, integrating geological structure data of the study area.The model size is 3000m×400m, including normal fault, reverse fault and fracture zone. Due to the tensile and shear resistance of loess soil [30], several cracks are also designed near the fault (Fig. 6). The vP of the first layer is 600m/s, the vP of the second layer is 1200m/s, the vP of the third layer is 1800m/s, the vP of the fourth layer is 2400m/s, the velocity of the fracture zone is 400m/s, and the velocity of the fracture zone is 300~350m/s. Single side shooting is used to collect seismic data. The channel spacing is 8m, 75 channels are received, the shot spacing is 24m, the maximum offset is 600m, the source wavelet is 35Hz Rayleigh wavelet, and the sampling interval is 1ms. A total of 100 shots of seismic records are collected.

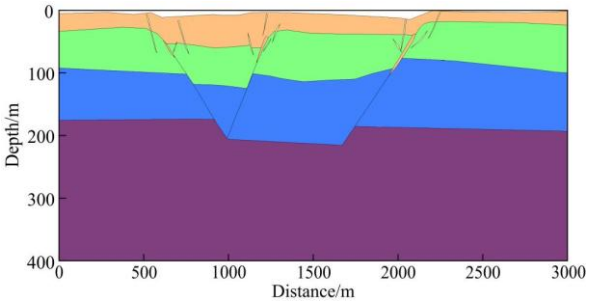

Fig 6 Fault Model

When seismic waves encounter faults and fracture points during propagation, they generate diffracted waves and scattered waves. When first-break waves pass through a fault interface and enter the strata on the opposite side, they undergo refraction due to velocity differences between the strata on either side, causing their propagation direction to deviate from the original path[14]. Figure 7 shows the seismic records of the 7th, 33rd and 64th shots in the forward modeling of the fault model, and the position and distortion of the fault influence are clearly shown in the black box. From the seismic records obtained by forward modeling, it can be seen that the fault has changed the propagation path of the first break wave. When the fault breakpoint is encountered in the propagation process, the waveform has changed, leading to the first break anomaly.

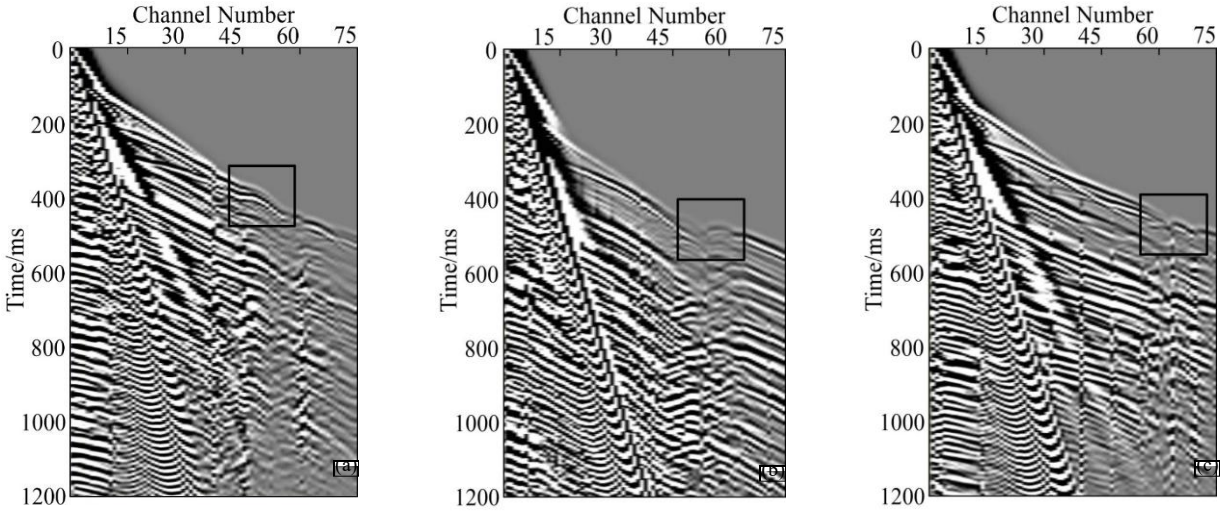

Fig. 7 Seismic Record of Fault Model

First-break tomography was applied to the simulated seismic records, with the inversion results presented in Figure 8. The tomography inversion results exhibit high overall consistency with the established 2D fault geological model, and the spatial correspondence between velocity anomaly zones and geological structures is relatively accurate. Faults manifest as velocity anomaly zones: the wave velocity of fault fracture zones is lower than that of the surrounding strata, and in the velocity structure image derived from tomography, fault zones exhibit obvious low-velocity anomalies.Through analysis of the tomography results, the location and strike of the faults can be roughly determined; furthermore, based on the intensity and extent of low-velocity anomalies, the width and fracture degree of fault fracture zones can be preliminarily inferred. However, it should be noted that the inversion results for multiple ground fissures in the geological model are poor: the exact location, strike, and width of individual ground fissures cannot be clearly identified in the inversion results, and only a vague low-velocity anomaly zone can be observed near the faults, making it difficult to distinguish the individual characteristics of multiple fissures.The main reasons are likely as follows: First, ground fissures are of small scale—far smaller than the wavelength of seismic wavelets in the loess layer-and the volume ratio of a single fissure is low. This results in a weak impact on first-break traveltime, making it difficult to generate independent, identifiable anomaly signals. Second, signal interference and masking occur: the signal intensity of strong low-velocity anomalies in faults and fracture zones is far greater than that of individual fissures, leading to the complete submergence of weak anomalies from fissures, which cannot be effectively separated. Additionally, due to the inherent non-uniqueness and resolution limitations of first-break tomography, there remain certain errors and uncertainties in the accurate characterization and parameter inversion of anomaly zones. These require comprehensive analysis and verification in conjunction with other geophysical methods and geological data.

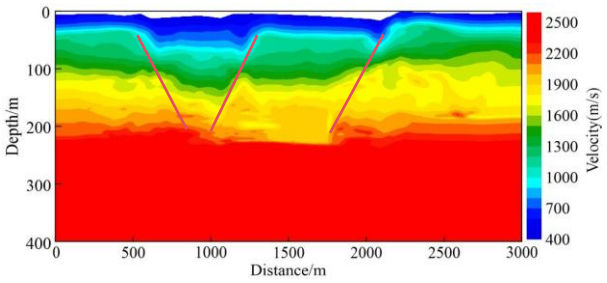

Fig. 8 Inversion Results of Fault Model

4.2. Actual Data Processing and Analysis

The study area is located in the western part of Fengxiang County. The exploration survey line (marked by the black line in Figure 1b) is approximately 18 km long and arranged across the Qianyang Fault. The terrain in this area exhibits stepped undulation, with the surface mainly covered by Quaternary loess; bedrock is only sporadically exposed along river channels and parts of valley bottoms. The shallow seismic-geological structure shows significant lateral variations and complex conditions.

Data acquisition was conducted using the Geometrics Model DZ-240 distributed seismic acquisition system, equipped with 28 Hz geophones and using a 20 kg drop-weight source for excitation. The acquisition parameters are as follows: recording length of 1.5 s, sampling interval of 0.25 ms, and fold coverage of 40. The observation system adopts 160-channel reception and is symmetrically arranged with intermediate shooting, with a shot point spacing of 8 m and a channel spacing of 4 m.

At the stage of first break picking and initial model establishment, the travel time data of first break wave is obtained based on shot set records (Fig. 9). Velocity structure parameters are determined by combining the characteristics of refracted seismic time-distance curves and traveltime inflection point analysis, and the top interface of the model is set to the actual topographic surface by integrating surface elevation data. To ensure calculation accuracy and inversion convergence rate, the initial model is configured with the following parameters: maximum depth of 300 m, top interface aligned with the survey line elevation, velocity block grid unit of 2 m × 1 m, and geophone point elevation ranging from 730–1200 m. During traveltime inversion, after 10 iterations of the loaded first-arrival data, the root mean square error (RMSE) decreases from 72 ms in the first iteration to approximately 15 ms in the second, and finally stabilizes at 12 ms. The original first-arrival traveltimes are in good agreement with the theoretical traveltimes of the inverted model, and the inversion results are presented in Figure 10. As shown in the ray density map (Figure 10a), the horizontal coverage is uneven: the detection depth ranges from 50–200 m, with overall good coverage; local ray coverage reaches 80–200 times, while only approximately 50 times coverage is achieved at the north and south ends of the survey line due to limitations of the observation system. Through comprehensive assessment, the velocity model in the effective ray coverage area (especially the shallow layer of 0–180 m) exhibits high reliability, which can provide a basis for shallow surface structure analysis. It is suggested that the velocity parameters in ray-sparse areas should be comprehensively interpreted in combination with geological prior information to improve the scientific rigor of the results.

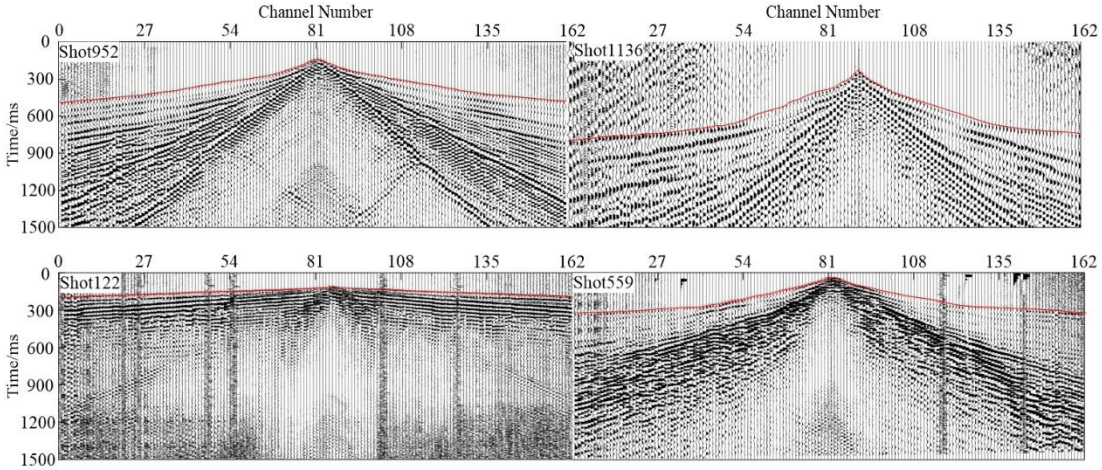

Fig. 9 Actual Seismic Data (Red in the Figure is the Picked Travel Time Information)

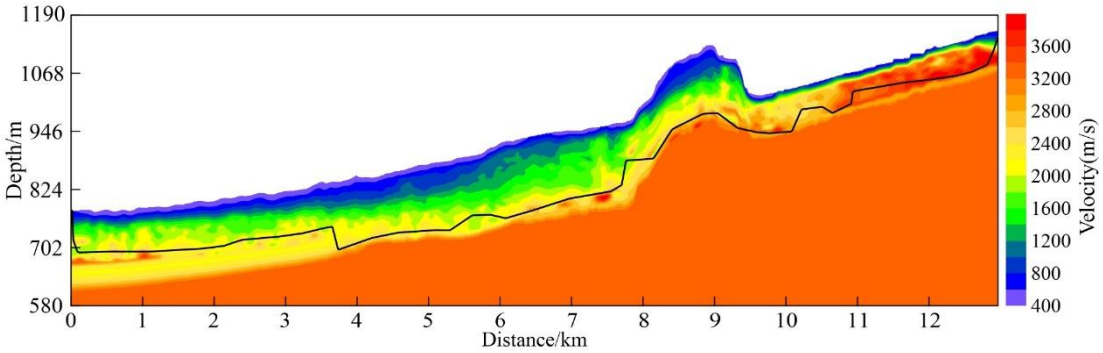

(a) Lateral Inversion Ray Coverage Density

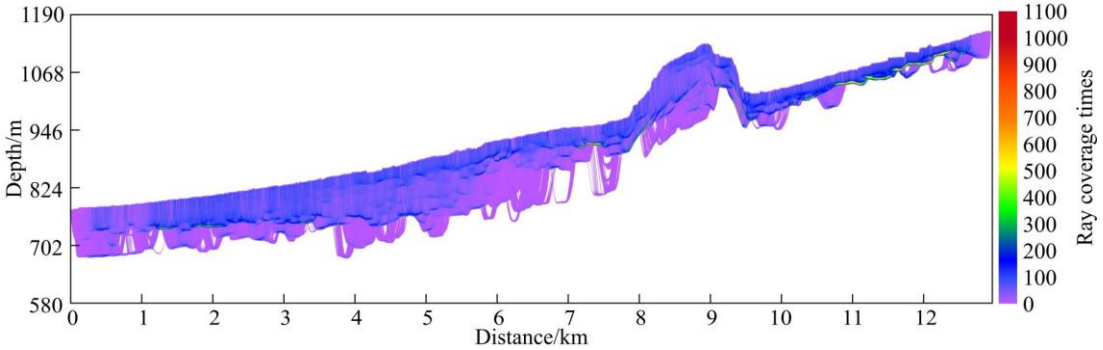

(b) Lateral Inversion Inversion Results

Fig. 10 Velocity Structure of Loess Retrieved Along the Actual Data Profile

4.2.1. Velocity structure analysis of loess layer

To comprehensively analyze the shallow geological structure and velocity characteristics, this study conducts joint interpretation of the first-break tomography inversion results by integrating reflection imaging results. The velocity section obtained from inversion is presented in Figure 10b, where the gray line marks the bottom interface of tomographic ray density. The results show that the overall velocity structure of the section exhibits a characteristic of being lower in the south and higher in the north, with significant variations in the lateral velocity gradient. This trend is largely consistent with the geological conditions detected by Wang Qiuyu (2019) during geological mapping in the Baoji Area, and highly consistent with the research results of Li Wenhui (2022) in the northern margin of the Weihe Basin.

Due to the control of differences in formation lithology, density, and water content, the propagation velocity of seismic waves in loess media exhibits an obvious stratified effect, with the velocity of the near-surface loess layer increasing linearly with depth. In the locally enlarged section at the horizontal 3–4 km (Fig. 11a), the three velocity interfaces (600 m/s, 1200 m/s, and 1800 m/s) are clear and continuous, and the stratification is particularly prominent. Based on this, the fine division of the loess layer can be completed: along the 0–9 km range of the survey line, the 0–180 m depth in the shallow part of the basin is dominated by low-velocity characteristics (<1800m/s); vertically, it develops a 0–30 m thick loose air-dried loess layer, a 10–50 m thick moist loess layer, and a 20–50 m thick clayey layer. Additionally, the thickness of the clayey layer increases from the north to the bottom of the mountain. The 9–12 km section of the survey line features a typical loess gully landform; affected by the superimposed influence of long-term water erosion and gravitational action, the thickness of the surface loess layer decreases sharply (with a maximum thickness of only 20 m) and is in direct contact with the bedrock weathering crust. Furthermore, two concealed faults (F1 and F2) were jointly identified by the velocity section and reflection section: Fault F1 is located in the middle of the survey line (approximately 7–8 km), with an attitude of nearly vertical. The velocity section shows it as a low-velocity fractured zone with a width of approximately 50–80 m. In the reflection section (Fig.

11b), the continuity of the corresponding T wave group is interrupted, accompanied by small-scale diffracted waves, which is inferred to have been formed by regional compressive stress. Fault F2 is distributed in the northern section of the survey line and is part of the Qianyang Fault. On the velocity section, it is characterized by the obvious uplift of deep high-velocity bedrock and a sudden change in lateral velocity.

4.2.2. Analysis of loess bedrock interface

Based on the first-break tomographic inversion results, and using the 1800 m/s velocity contour as the core identification marker, the unconformable contact interface between the loess layer and the underlying bedrock can be clearly defined. This interface is largely coincident with a set of highly continuous strong reflection wave groups (T wave groups) in the reflection profile, which is inferred to be the Cenozoic basal interface. Several high-velocity anomalous bodies with irregular shapes are developed below this interface, with velocities significantly higher than that of the overlying loess layer. Combined with the regional sedimentary background and lithological characteristics, these bodies are inferred to be medium-dense to dense gravelly soil layers of pluvial origin, mainly composed of limestone fragments and calcareous cemented gravel. The topography of the Cenozoic basal interface in this area is relatively gentle, generally showing a trend of being higher in the north and lower in the south. However, the surface of this area is a typical loess tableland with crisscross gullies, resulting in significant variations in the thickness of the Cenozoic loess. The 0-180 m depth in the shallow part of the basin generally exhibits low-velocity characteristics (<1800m/s), corresponding to the widely distributed Quaternary aeolian loess and alluvial-pluvial loose sediments. In contrast, an obvious zone of steep velocity gradient change occurs in the northern uplift area, where the velocity rapidly increases to over 2000 m/s. This reveals the geological process in which the basement rock mass is eroded due to tectonic uplift, and the thickness of the loess cover is significantly reduced. This "velocity-lithology" coupling model is mutually corroborated with the strong reflection signals and undulating morphology of the bedrock top boundary in the reflection seismic data. A geological model was constructed via the velocity section and reflection section (Fig. 12), which effectively improves the reliability of the interpretation results. This provides technical support and valuable insights for the identification of concealed interfaces, lithological division, and high-precision geological mapping in loess-covered areas.

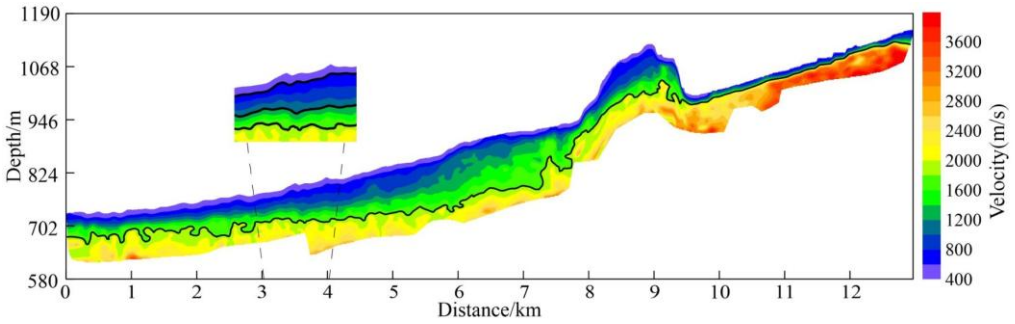

(a) Velocity Profile Interpretation

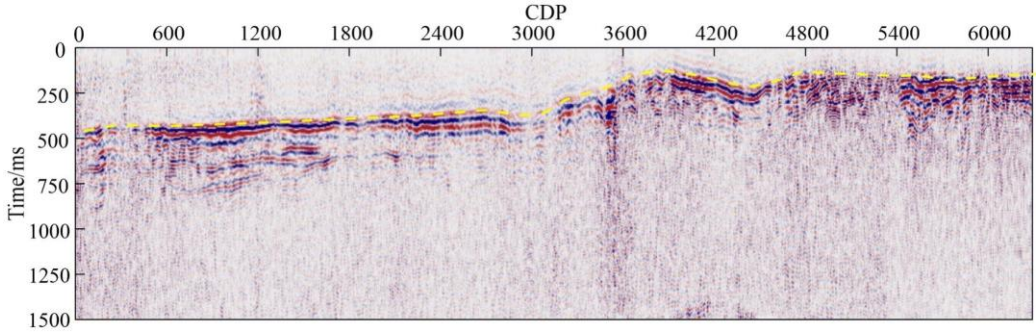

(b) 2D Reflection Seismic Imaging Profile

Fig. 11 Interpretation of Actual Data

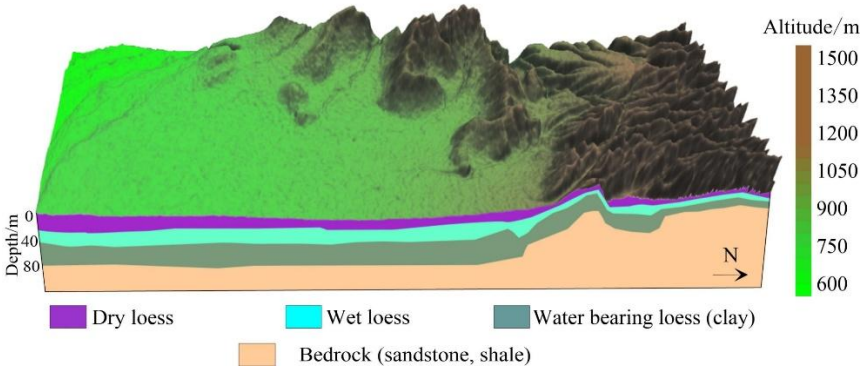

Fig. 12 loess geological model

5. CONCLUSION

Taking the loess layer in Qianyang area as the research object, the applicability and effectiveness of first break tomography technology in the detection of loess layer structure are systematically explored by combining theoretical analysis, forward modeling and practical data application

(1) Through the investigation and analysis of geological data, the vertical stratification law and horizontal distribution characteristics of the loess layer in the study area were clarified, and the key parameters of each layer were obtained. Using these basic parameters, an initial geological-geophysical model reflecting the macro-structural characteristics of the loess layer in the study area was constructed, providing a basic framework for subsequent technical applications.

(2) Based on the constructed initial model, multiple typical loess layer geological models—such as those with a horizontal surface, undulating surface, and faults—were designed to conduct forward modeling. The modeling results show that topographic relief causes the bending of seismic wave propagation paths, leading to regional offsets of first-arrival travel times; faults and fracture zones trigger seismic wave diffraction, resulting in local disorder of first-break signals and travel time distortion. The inversion results based on these influences indicate that first-break tomography technology can effectively overcome the aforementioned issues, accurately capturing the velocity differences and spatial morphologies of different loess layers. Comprehensive forward modeling results confirm that this technology can adapt to the complex near-surface conditions in loess tableland areas and exhibits good applicability in loess layer structure detection.

(3) First-arrival travel time data in the study area were used to conduct tomographic inversion; combined with the comprehensive interpretation of seismic reflection profiles, the fine structure, thickness variations, and horizontal distribution patterns of the underground loess layer were clearly identified. Additionally, the locations and morphologies of the loess-bedrock interface, internal loess interfaces, and hidden fault interfaces were accurately recognized.

REFERENCES

[1] Han L.H., Hu Z.D., Di B.R., et al. Numerical Simulation and Propagation Law of Seismic Wavefield in the Loess Plateau Area of the Ordos Basin [J]. Oil Geophysical Prospecting, 2024, 59(3): 504-513.

[2] Zheng L., Ji L.S., He Z.X., et al. Application Effect of Comprehensive Geophysical Exploration Technology in the Loess Plateau Area of the Western Ordos Basin [J]. Oil Geophysical Prospecting, 2008, (2): 229-232+128.

[3] Shen H.Y., Wang X., Li X.X. Review on Near-Surface Structure Survey and Parameter Inversion [J]. Petroleum Geophysical Prospecting, 2019, 58(4): 471-485+540.

[4] Sun P.P., Zhang M.S., Cheng X.J., et al. Occurrence Law of Geological Hazards on the Loess Plateau [J]. Journal of Mountain Science, 2019, 37(5): 737-746.

[5] Jiang Y.L., Zhang C.X., Huang X. Application of High-Density Resistivity Method in Detecting the Thickness of Overburden for Hydropower Station Site Selection [J]. Computing Techniques for Geophysical and Geochemical Exploration, 2008, (3): 235-238+171.

[6] Hu Z.Z., Shi Y.L., He Z.X., et al. Application of Transient Electromagnetic Method in Loess Layer Exploration in Western China [J]. Oil Geophysical Prospecting, 2016, 51(S1): 131-136+10.

[7] Shan B., Wang Y.H., Hou S.G. Comprehensive Application of Multi-Channel Transient Surface Wave and Natural Source Surface Wave Exploration Methods in Filled Areas [J]. Geotechnical Investigation & Surveying, 2017, 45(S2): 311-315.

[8] Zhang J.H., Wang L., Wang X.Y., et al. Application Study of Microtremor Exploration in Loess Stratigraphic Division [J]. Journal of Taiyuan University of Technology, 2025, 56(3): 567-573.

[9] Wen X.K., Liu S., Li S.Q., et al. Application of Tomography in Near-Surface Structure Survey in the Loess Plateau Area [J]. Geophysical and Geochemical Exploration, 2012, 36(5): 766-771.

[10] Wang L.H., Liang J.L., Peng L.Y. Application of First-Arrival Wave Tomography in Concealed Fault Detection [J]. CT Theory and Applications, 2015, 24(1): 29-36.

[11] Yu D., Sun Y., Lu J., et al. Parallel Algorithm of Shallow First-Arrival Wave Traveltime Tomography and Its Application in Ground Fissure Survey [J]. Geophysical and Geochemical Exploration, 2017, 41(5): 977-985.

[12] Li F.Y., Kang P., Liu Y.P., et al. First-Arrival Wave Traveltime Tomographic Inversion of Marine Towed Cable Seismic Data [J]. CT Theory and Applications, 2018, 27(2): 197-204.

[13] Zhang X.Q., Liu Z.D., Liu Y.L., et al. Near-Surface Forward Modeling and Constrained Tomographic Inversion in the Ultra-Thick Loess Plateau [J]. Computing Techniques for Geophysical and Geochemical Exploration, 2022, 44(5): 539-547.

[14] Sun M.R., Ding X., Shi C., et al. Study on Seismic Wavefield Response Characteristics of Near-Surface Concealed Faults and Application of First-Arrival Wave Imaging [J]. Geology and Exploration, 2023, 59(5): 1043-1053.

[15] Wang J.Q., Jia N., Liu C.Y., et al. Gravel Assemblage Analysis of Conglomerate in the Yijun Formation of Lower Cretaceous in the Southwestern Ordos Basin and Its Significance [J]. Acta Sedimentologica Sinica, 2011, 29(2): 226-234.

[16] Li Y.H., Gao Z.L. Characteristics, Hazards and Control of Soil and Water Loss in the Loess Plateau Area [J]. Ecological Economy, 2011, (8): 148-153.

[17] Shi P.P., Xiao A.C., Fu J.H., et al. Sedimentary Tectonic Framework and Evolution of the Ordovician Foreland Basin in the Southern Margin of the Ordos Block [J]. Acta Petrologica Sinica, 2021, 37(8): 2531-2546.

[18] Zhang Y.Q., Han M.T., Cao J.P., et al. Study on Current Crustal Deformation and Tectonic Characteristics of the Weihe Basin and Its Adjacent Areas [J]. China Earthquake Engineering Journal, 2021, 43(1): 79-89.

[19] Xi Z. Numerical Simulation and Case Study of Seismic Wavefield in the Loess Plateau Area [D]. Xi'an: Xi'an University of Science and Technology, 2010.

[20] Tan C.X., Sun W.F., Zhang C.S., et al. Study on Engineering Geological Characteristics of Drilled Cores from Typical Loess Profiles in Baoji Area [J]. Journal of Engineering Geology, 2011, 19(5): 732-748.

[21] Wang Y., Sun H.Y., Tian M.Z. Correlation and Subdivision of Loess Strata on the Loess Plateau [J]. Geological Journal of China Universities, 2015, 21(2): 346-356.

[22] Wang D.X., Du Z.D., Zhang M.B., et al. Investigation and Analysis of Geophysical Characteristics of Shallow Loess in the Ordos Basin. In: Proceedings of the 2017 China Union of Geoscience Meetings (31), 2017: 75-77.

[23] Shao G.Z., Li Y.L., Yue L. Application of Joint Exploration of Active Source and Passive Source Surface Waves in 3D Imaging of Loess-Covered Areas [J]. Geophysical and Geochemical Exploration, 2022, 46(4): 897-903.

[24] Han L.H., Sun Z.Q., Hu Z.D., et al. First-Arrival Traveltime Calculation and Characteristic Analysis of Variable-Density Unequally Spaced Grids in 3D Complex Loess Plateau Areas [J]. Chinese Journal of Geophysics, 2022, 65(8): 3108-3122.

[25] Yu J. Sedimentary Environment and Tectonic Significance of the Early Cretaceous Yijun Formation in the Southwestern Margin of the Ordos Basin [D]. Xi'an: Chang'an University, 2018.

[26] Li Q.Z. The Road to Precise Exploration. Beijing: Petroleum Industry Press, 1993: 35-38.

[27] Wu G.W., Xiong X.S., Gao R., et al. 2D First-Arrival Wave Tomography of the Upper Crust in the Southern Part of the Beishan Tectonic Belt [J]. Earth Science Frontiers, 2022, 29(2): 402-415.

[28] Wang G., Xiong X.S., Lu Z.W., et al. Shallow Crustal Structure of the Lanping Basin - Western Margin of the Yangtze Block Revealed by 2D First-Arrival Wave Tomography [J]. Acta Geoscientica Sinica, 2024, 45(6): 989-1001.

[29] Liang Y., Gu H.M., Li C., et al. Numerical Simulation of Seismic Wave Excitation and Wavefield Characteristics in the Slope Zone of the Loess Plateau [J]. Science Technology and Engineering, 2019, 19(22): 70-75.

[30] Liu C., Qiao J.W., Peng J.B., et al. Basic Characteristics and Genetic Analysis of Ground Fissures in Anren Town, Weihe Basin [J]. Journal of Engineering Geology, 2022, 30(1): 242-253.

[31] Wang Q.Y. Study on Geophysical Mapping Methods in Loess-Covered Areas [D]. Xi'an: Chang'an University, 2019.

[32] Li W.H., Wang H.Y., Gao R., et al. Study on Fine Velocity Structure of the Upper Crust in the Qinling Orogenic Belt and Its Adjacent Areas [J]. Earth Science Frontiers, 2022, 29(2): 198-209.